

# Stabilizing Single-Atom and Small-Domain Platinum via Combining Organometallic Chemisorption and Atomic Layer Deposition

Shengsi Liu,<sup>†,⊥</sup> J. Miles Tan,<sup>†,⊥</sup> Ahmet Gulec,<sup>‡</sup> Lawrence A. Crosby,<sup>‡,Ⓛ</sup> Tasha L. Drake,<sup>†</sup> Neil M. Schweitzer,<sup>§</sup> Massimiliano Delferro,<sup>†,Ⓢ</sup> Laurence D. Marks,<sup>‡</sup> Tobin J. Marks,<sup>\*,†,Ⓛ</sup> and Peter C. Stair<sup>\*,†,Ⓛ</sup>

<sup>†</sup>Department of Chemistry and the Center for Catalysis and Surface Science, Northwestern University, 2145 Sheridan Road, Evanston, Illinois 60208, United States

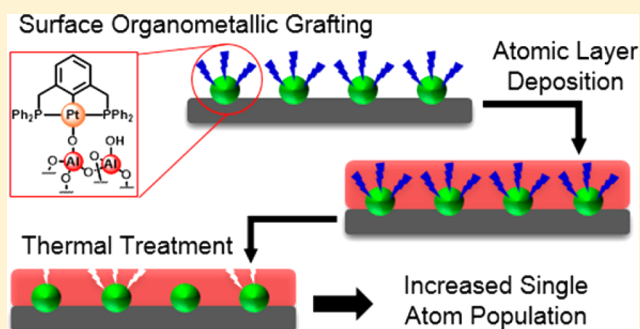
<sup>‡</sup>Department of Materials Science and Engineering and the Center for Catalysis and Surface Science, Northwestern University, 2145 Sheridan Road, Evanston, Illinois 60208, United States

<sup>§</sup>Department of Chemical and Biological Engineering and the Center for Catalysis and Surface Science, Northwestern University, 2145 Sheridan Road, Evanston, Illinois 60208, United States

<sup>Ⓛ</sup>Chemical Sciences and Engineering Division, Argonne National Laboratory, 9700 S. Cass Avenue, Lemont, Illinois 60439, United States

## Supporting Information

**ABSTRACT:** Oxide-supported single-atom Pt materials are prepared by combining surface organometallic chemisorption with atomic layer deposition (ALD). Here Pt is supported as a discrete monatomic “pincer” complex, stabilized by an atomic layer deposition (ALD) derived oxide overcoat, and then calcined at 400 °C under O<sub>2</sub>. ALD-derived Al<sub>2</sub>O<sub>3</sub>, TiO<sub>2</sub>, and ZnO overlayers are effective in suppressing Pt sintering and significantly stabilizing single Pt atoms. Furthermore, this procedure decreases the overall Pt nuclearity (~1 nm average particle diameter) versus bare Pt (~3.8 nm average diameter), as assayed by aberration corrected HAADF-STEM. The TiO<sub>2</sub> and ZnO overcoats are significantly more effective at stabilizing single-atom Pt species and decreasing the overall Pt nuclearity than Al<sub>2</sub>O<sub>3</sub> overcoats. Vibrational spectroscopy of adsorbed CO also shows that oxidized Pt species commonly thought to be single Pt atoms are inactive for catalytic oxidation of adsorbed CO. CO chemisorption measurements show site blockage by the ALD overcoats.



## INTRODUCTION

The study of isolated, supported late-transition-metal single-atom heterogeneous catalysts has recently become an area of intense research interest due to recent promising applications in catalytic CO oxidation,<sup>1–6</sup> methanol steam re-forming,<sup>7–9</sup> selective alcohol oxidation,<sup>10</sup> ethanol dehydration,<sup>11</sup> olefin and alkyne hydrogenation,<sup>12–16</sup> and the water-gas shift reaction,<sup>17–28</sup> as well as in other transformations.<sup>29–36</sup> Despite this rapid progress, the synthesis of such catalysts is not well-controlled or general. Known approaches include utilizing highly reducible supports,<sup>1,4,6,17,29,30,32</sup> supports with high defect densities,<sup>2,10,37,38</sup> addition of alkali-metal and f-element dopants,<sup>3,19,21,22,39</sup> cyanide-based metal leaching protocols,<sup>20,22,28,40</sup> and introduction of strongly binding N,S donor atoms into the support.<sup>12,35,41</sup> Considering both the recent and projected future growth of this promising area of science and technology, it is of interest to explore rational and generalizable methods for synthesizing such single-atom species. The primary challenges in such a synthetic effort are to deposit the late-transition-metal atoms on moderate-surface-area oxide supports

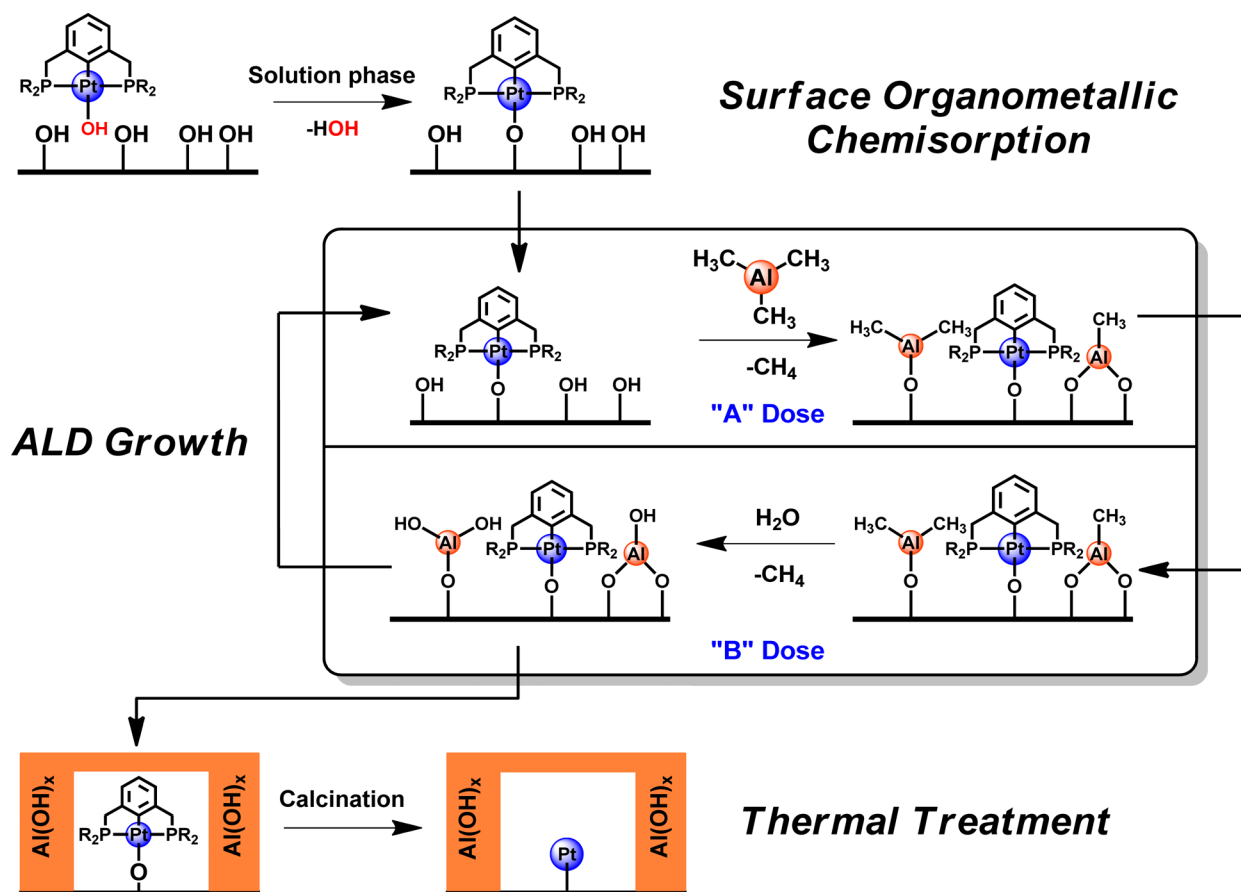
as monatomic species and to then develop strategies that mitigate sintering, even under high-temperature oxidative calcination. Furthermore, such methods should be applicable to supports that do not have high surface areas or high defect densities, since atomic isolation of metal atoms at extremely low surface densities is kinetically favorable.

There are a number of available strategies for depositing well-defined monatomic late-transition-metal species onto oxide supports. These include metal evaporation, “soft landing”,<sup>42–44</sup> and the chemisorption of intact organometallic species.<sup>45–80</sup> Of these approaches, organometallic chemisorption was chosen here due to its ability to deliver well-defined metal precursors to high-surface-area supports with uniform nuclearity. Paired with a strategy for mitigating sintering, a robust synthetic procedure can be envisaged whereby deposited Pt organometallic complexes remain monatomic even upon high-temperature thermal treatment and ligand removal.

Received: November 18, 2016

Published: February 7, 2017

Scheme 1. Overall Schematic for Proposed Single Pt Atom Synthetic Methodology Combining Surface Organometallic Chemisorption and ALD Approaches



ALD overcoating is a highly effective method for suppressing nanoparticle agglomeration and could conceivably be used to stabilize single atoms. Recently, it has been shown that Pd nanoparticles can be protected from sintering by overcoating with ALD-derived Al<sub>2</sub>O<sub>3</sub>. The resulting material does not exhibit observable thermal sintering on heating to 500 °C and under ethane oxidative dehydrogenation (ODH) conditions at 600 °C,<sup>81–83</sup> whereas control samples without the ALD overcoats exhibit extensive particle agglomeration under identical conditions. In addition to the stability imparted to these nanoparticles, the ALD methodology offers the advantage of selectively depositing variable numbers of oxide overcoat layers even under thermally mild conditions (50 °C),<sup>84–90</sup> which should prevent premature thermal decomposition of deposited organometallic species. This approach has been utilized by other research groups, although the overcoats were not necessarily based by ALD.<sup>91–101</sup>

Recent work in this laboratory has shown that highly dispersed low-coordinate Pd sites can be efficiently prepared by surface organometallic chemisorption.<sup>102</sup> Since low coordination of metal centers can only be fully achieved when they are atomically dispersed,<sup>36</sup> we envisioned that, by combining this methodology with ALD, the synthesis of oxide-supported single-atom catalysts could be explored in a rational fashion. Here we report a synthetic approach to stabilizing Pt single atoms on Al<sub>2</sub>O<sub>3</sub> by combining surface organometallic chemisorption with ALD techniques (Scheme 1). First, the complex (P<sup>h</sup>PCP)Pt-OH is chemisorbed on Al<sub>2</sub>O<sub>3</sub> from solution. The resulting material is next overcoated with oxide

layers by ALD to suppress agglomeration and then calcined under flowing O<sub>2</sub> at 400 °C to remove the ancillary ligands. The final materials are then characterized by aberration-corrected HAADF STEM (AC-HAADF STEM), CO adsorption/diffuse reflectance infrared Fourier transform spectroscopy (DRIFTS), and XPS.

## RESULTS

**(P<sup>h</sup>PCP)Pt-OH Chemisorption.** The organometallic precursor (P<sup>h</sup>PCP)Pt-OH was selected for this study for both the kinetically robust coordination offered by the PCP ligand and the air stability of the resulting Pt-OH complex (Scheme 1).<sup>103</sup> Moreover, (P<sup>h</sup>PCP)Pt-OH contains ligand framework P atoms which allow tracking the state of the supported complex during the chemisorption, ALD, and calcination processes by <sup>31</sup>P CPMAS solid-state NMR spectroscopy. (P<sup>h</sup>PCP)Pt-OH is also a good precursor candidate due to its protonolytic reactivity.<sup>104</sup> Analogous complexes such as (P<sup>h</sup>PCP)Pd-OH are known to exchange the -OH ligand with alcohols to yield alkoxides.<sup>105,106</sup> Upon reaction of the Al<sub>2</sub>O<sub>3</sub> powder with a benzene-*d*<sub>6</sub> solution of the precursor, adsorption of a significant amount of the precursor is observed in the solution-phase <sup>1</sup>H NMR, with no evidence of Al<sub>2</sub>O<sub>3</sub>-induced decomposition (Figure S1 in the Supporting Information). This indicates that the precursor is indeed bound to the Al<sub>2</sub>O<sub>3</sub> surface. Further evidence of successful chemisorption is indicated by solution-phase and solid-state CPMAS <sup>31</sup>P NMR studies. The <sup>31</sup>P chemical shift in benzene-*d*<sub>6</sub> of the P centers in the intact (P<sup>h</sup>PCP)Pt-OH complex is observed at δ 30 ppm (Figure 1A).

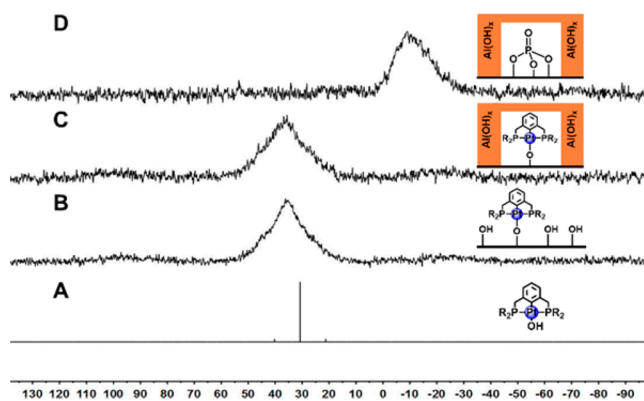


**Figure 1.** (A)  $^{31}\text{P}$  NMR spectrum of  $(^{\text{Ph}}\text{PCP})\text{Pt-OH}$  (400 MHz,  $\text{C}_6\text{D}_6$ ). (B–D)  $^{31}\text{P}$  CPMAS solid state NMR stackplot spectra (MAS rate, 10 kHz; contact time, 5 ms; recycle delay time, 5 s; NS, 5000 scans) of (B)  $(^{\text{Ph}}\text{PCP})\text{Pt-Al}_2\text{O}_3$  without calcination, (C) 20Al- $(^{\text{Ph}}\text{PCP})\text{Pt-Al}_2\text{O}_3$  prior to calcination, and (D) 20Al- $(^{\text{Ph}}\text{PCP})\text{Pt-Al}_2\text{O}_3$ -400 cal (Pt omitted for clarity).

In comparison, a similarly positioned peak at  $\delta$  35 ppm is observed in solid-state CPMAS  $^{31}\text{P}$  NMR of  $(^{\text{Ph}}\text{PCP})\text{Pt-Al}_2\text{O}_3$  (Figure 1B), arguing that the  $(^{\text{Ph}}\text{PCP})\text{Pt-O-}$  framework is indeed intact. Thus, similarly sized  $^{31}\text{P}$  NMR shifts of surface-bound organometallics relative to those of the corresponding intact solution-phase precursors were previously observed by Alper in studies of Pd phosphine complexes supported on  $\text{SiO}_2$ .<sup>107</sup> The present resonance has a full-width at half-maximum of approximately 2250 Hz. This is attributed to overlap of the main isotropic resonance with  $^{195}\text{Pt}$  satellites that arise from  $^1J_{\text{Pt-P}}$  scalar coupling. For reference, the magnitude of  $^1J_{\text{Pt-P}}$  scalar coupling reported by Bennett et al. for the intact  $(^{\text{Ph}}\text{PCP})\text{Pt-OH}$  was approximately 3064 Hz.<sup>103</sup> Scalar  $J_{\text{Pt-P}}$  coupling in the solid state has also been observed by other researchers.<sup>59,108–110</sup> Despite repeated toluene washes in the synthetic procedure, the present Pt species remain immobilized on the oxide support, arguing for chemisorption rather than physisorption. On the basis of this evidence, it is likely that the chemisorption process proceeds via protonolytic exchange with  $\text{Al}_2\text{O}_3$  support hydroxyl protons, as depicted in Scheme 1.

**Stability of the Supported Organometallic Complex under ALD and Calcination Conditions.** The stability of the supported Pt complex against reductive decomposition under ALD conditions was first examined. Various decomposition pathways are conceivable, since several of the ALD precursors used in this study contain polarized alkyl groups or strongly donating anionic ligands which might alkylate and/or reduce the  $(^{\text{Ph}}\text{PCP})\text{Pt-Al}_2\text{O}_3$  complex. Thus, all ALD experiments were carried out at 50 °C to minimize thermally induced decomposition. The consequences of the ALD overcoating were assessed by solid-state  $^{31}\text{P}$  NMR spectroscopy of the freshly  $\text{Al}_2\text{O}_3$  overcoated (20 cycles) material acquired under the same conditions as for the uncoated sample.

As shown in Figure 1C, the  $^{31}\text{P}$  chemical shift remains essentially unchanged. Upon high-temperature (400 °C) treatment under  $\text{O}_2$ , a new peak at  $\delta$  -15 ppm is observed, indicating the formation of oxidized phosphate species on the  $\text{Al}_2\text{O}_3$  surface.<sup>111–113</sup> Therefore, even after ALD,  $\text{O}_2$  is still able to access the  $(^{\text{Ph}}\text{PCP})\text{Pt-Al}_2\text{O}_3$  species and oxidatively decompose the  $^{\text{Ph}}\text{PCP}$  ligand. Analogously, the same experiments were performed with  $\text{TiO}_2$  and  $\text{ZnO}$  overcoats and

similar results are observed (Figures S2 and S3 in the Supporting Information).

**AC-HAADF-STEM Study.** Images of large areas of uncalcined  $(^{\text{Ph}}\text{PCP})\text{Pt-Al}_2\text{O}_3$  taken by HAADF-STEM (without aberration correction) show no evidence of nanoparticle formation (Figure S4 in the Supporting Information). Higher magnification images obtained by AC-HAADF-STEM (Figure 2A) reveal the presence of single Pt atoms and the absence of nanoparticles, although electron-beam-induced mobility, a common phenomenon in such experiments, was observed.<sup>114–118</sup> In some cases, for example, images taken of the same area reveal different spatial arrangements of single atoms. This is consistent with Pt remaining as an isolated organometallic species upon supporting on  $\text{Al}_2\text{O}_3$ . After calcination at 400 °C,  $(^{\text{Ph}}\text{PCP})\text{Pt-Al}_2\text{O}_3$  exhibits significant sintering, and Pt nanoparticles up to 10 nm in size are observed.

However, a detailed particle count reveals that the majority of the observed Pt species are single atoms. Specifically, on the basis of the TEM images (Figure 2B), ca. 70% of the imaged Pt species are in single-atom form, while particles up to 10 nm are also observed. In order to obtain a meaningful analysis of the sizes of the nanoparticles observed in each sample, particle size distributions were obtained by analyzing the nanoparticle Pt domains (i.e., all Pt domains that were not in single atom form). In this nomenclature, each instance of physically isolated Pt cluster or nanoparticle is counted as one domain. Thus, after calcination, in addition to single Pt atoms,  $(^{\text{Ph}}\text{PCP})\text{Pt-Al}_2\text{O}_3$  forms nanoparticles that are 3.8 nm in diameter on average, with particles as large as 10 nm observed as well.

For the  $\text{Al}_2\text{O}_3$ -overcoated sample, sintering is once again evident and particles up to ca. 10 nm are observed by AC-HAADF-STEM (Figure 2C). As in the previous nonovercoated samples, ca. 70% of the imaged Pt species are in single-atom form. However, an analysis of the nanoparticle fraction of the Pt species (Figure 3) shows that the ALD  $\text{Al}_2\text{O}_3$  overcoats are modestly effective at reducing the average particle size. This is in agreement with previous studies showing that ALD  $\text{Al}_2\text{O}_3$  overcoats selectively block reactive edges and corner sites to stabilize small 1–2 nm Pd particles against thermal sintering.<sup>83</sup> However, because ALD overcoating in this study is performed prior to decomposition of the Pt precursor to nanoparticles, it is unclear if this mechanism is operative here. The dispersion of the present supported Pt species can also be increased by adding a more reducible metal oxide phase. This approach has been previously exploited to stabilize small Pt nanoparticle domains,<sup>91–101</sup> and it is known that the sintering rates of single-atom Pt are support dependent and that supports which interact more strongly with Pt can significantly inhibit sintering.<sup>119,120</sup> Thus, studies were performed here in which  $(^{\text{Ph}}\text{PCP})\text{Pt-Al}_2\text{O}_3$  was overcoated with an oxide other than  $\text{Al}_2\text{O}_3$  with the goal of introducing a phase that interacts differently with Pt in comparison to the support. In this case, both  $\text{ZnO}$  and  $\text{TiO}_2$  overcoats were investigated by employing well-established procedures<sup>84–90</sup> to target similar overcoat thickness compared to the  $\text{Al}_2\text{O}_3$ -coated sample for a fair comparison across samples.

For  $(^{\text{Ph}}\text{PCP})\text{Pt-Al}_2\text{O}_3$  centers overcoated with  $\text{ZnO}$  and  $\text{TiO}_2$ , followed by calcination under  $\text{O}_2$  at 400 °C, no nanoparticles significantly larger than 2 nm are observed, implying a significant stabilizing effect. Particle size distributions, with the single-atom fraction excluded, are shown in Figure 3. As can be seen for the overcoated samples, the vast

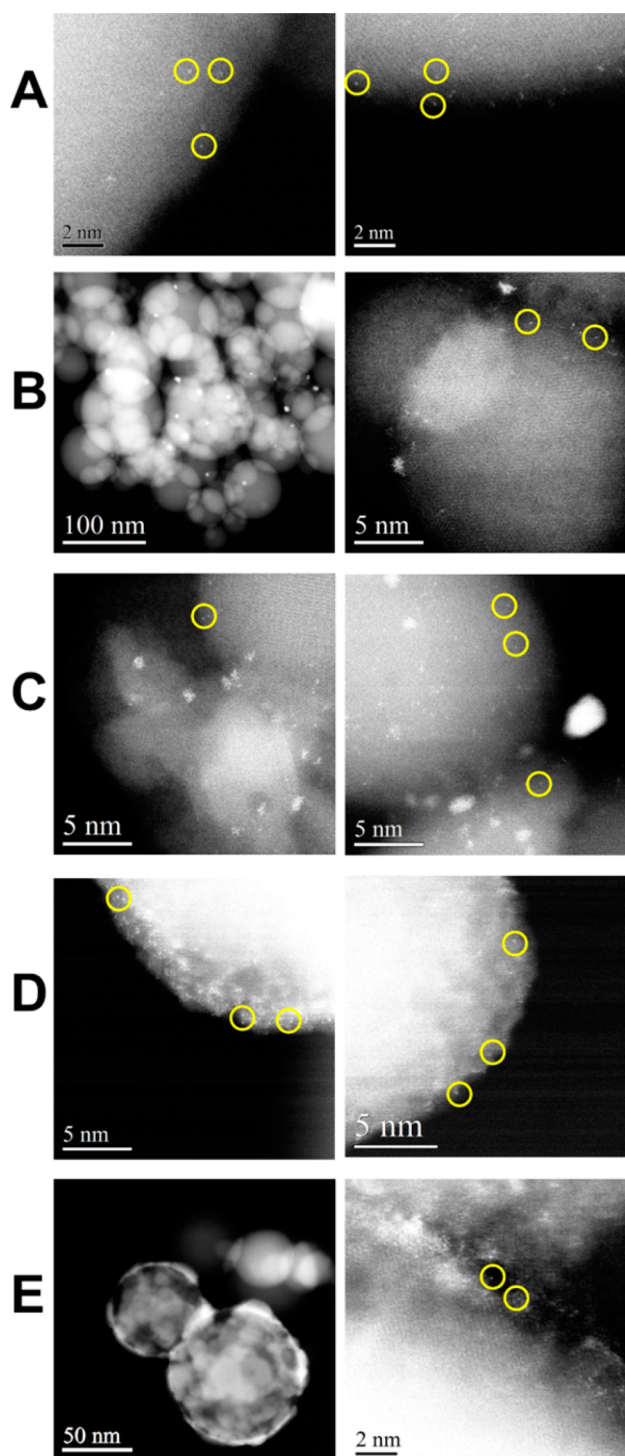


**Figure 2.** HAADF images of (A)  $(^{\text{Ph}}\text{PCP})\text{Pt-Al}_2\text{O}_3$  prior to calcination, (B)  $(^{\text{Ph}}\text{PCP})\text{Pt-Al}_2\text{O}_3-400$  cal, (C)  $20\text{Al-} (^{\text{Ph}}\text{PCP})\text{Pt-Al}_2\text{O}_3-400$  cal, (D)  $40\text{Ti-} (^{\text{Ph}}\text{PCP})\text{Pt-Al}_2\text{O}_3-400$  cal, and (E)  $20\text{Zn-} (^{\text{Ph}}\text{PCP})\text{Pt-Al}_2\text{O}_3-400$  cal. Select single atoms are encircled in yellow.

majority of nanoparticles are in the 0–2 nm size range. The overcoated samples also display universally lower mean particle sizes (ca. 1 nm).

Note, however, that the  $\text{TiO}_2$ - and  $\text{ZnO}$ -containing samples are not uniformly overcoated, as determined by AC-HAADF-STEM. The  $40\text{Ti-} (^{\text{Ph}}\text{PCP})\text{Pt-Al}_2\text{O}_3-400$  cal sample shows several discrete  $\text{TiO}_2$  nanoparticles, as well as possibly inhomogeneous  $\text{TiO}_2$  coatings on the  $\text{Al}_2\text{O}_3$  nanospheres

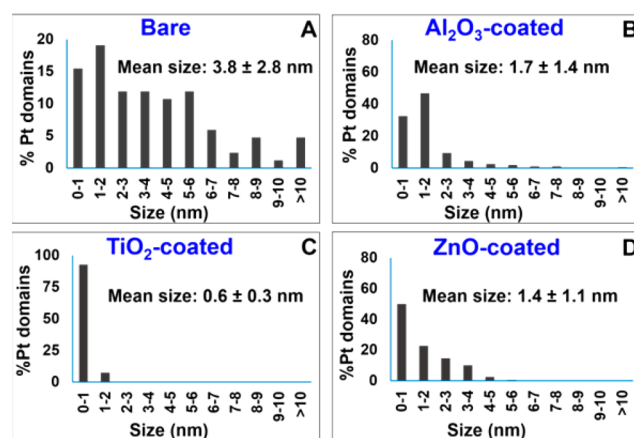


**Figure 3.** Particle size distributions (excluding single atoms) of (A)  $(^{\text{Ph}}\text{PCP})\text{Pt-Al}_2\text{O}_3-400$  cal, (B)  $20\text{Al-} (^{\text{Ph}}\text{PCP})\text{Pt-Al}_2\text{O}_3$ , (C)  $40\text{Ti-} (^{\text{Ph}}\text{PCP})\text{Pt-Al}_2\text{O}_3-400$  cal, and (D)  $20\text{Zn-} (^{\text{Ph}}\text{PCP})\text{Pt-Al}_2\text{O}_3-400$  cal. In this analysis, any physically isolated Pt cluster or nanoparticle counts as one “domain”, regardless of the size.

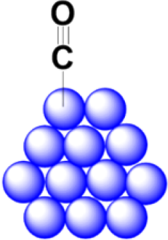

(Figure S5 in the Supporting Information). This behavior has been previously observed by de Resende, who prepared  $\text{TiO}_2$ -coated  $\text{Al}_2\text{O}_3$  supports by solution-phase methods. In that study, it was observed that at a sufficiently high weight loading, 33% of the surface density of  $\text{TiO}_2$  used in this study, anatase crystallites along with a surface coating were formed on the  $\text{Al}_2\text{O}_3$  support.<sup>121</sup> Similarly,  $\text{ZnO}$  domains are observed here on  $20\text{Zn-} (^{\text{Ph}}\text{PCP})\text{Pt-Al}_2\text{O}_3-400$  cal, and the overcoats are not of uniform thickness (Figure S5). EDS analysis of the “uncoated” domains in  $40\text{Ti-} (^{\text{Ph}}\text{PCP})\text{Pt-Al}_2\text{O}_3-400$  cal nevertheless shows deposition of varying, smaller amounts of  $\text{TiO}_2$  (Figure S6 in the Supporting Information). A weight-based distribution of the observed Pt species is also obtained. For this analysis, the percentage of Pt in single-atom form in each sample is estimated by obtaining the area density of single Pt atoms observed ( $(\text{atoms of Pt})/(\text{nm}^2 \text{ sample area})$ ) in high-magnification images by AC-HAADF-STEM. This number is then multiplied by the total sample area imaged by AC-HAADF-STEM at lower magnification, where nanoparticles and clusters, but not necessarily single atoms, are observable, to obtain an estimated count of single atoms present. The number of Pt atoms allocated to each nanoparticle observed is then estimated by assuming each has a hemispherical shape.<sup>122</sup>

This analysis shows that the quantity of Pt in single-atom form increases in the order  $(^{\text{Ph}}\text{PCP})\text{Pt-Al}_2\text{O}_3-400$  cal (5%) <  $20\text{Al-} (^{\text{Ph}}\text{PCP})\text{Pt-Al}_2\text{O}_3-400$  cal (18%) <  $20\text{Zn-} (^{\text{Ph}}\text{PCP})\text{Pt-Al}_2\text{O}_3-400$  cal (35%) <  $40\text{Ti-} (^{\text{Ph}}\text{PCP})\text{Pt-Al}_2\text{O}_3-400$  cal (>95%). Pt atom percentage distributions derived by this method are shown in Figure S7 in the Supporting Information. Although these percentages are estimates, as a metric they provide a pragmatic approach to evaluating the extent to which single atoms are stabilized by the ALD overcoating materials used in this study. It should also be noted, however, that for the  $20\text{Zn-} (^{\text{Ph}}\text{PCP})\text{Pt-Al}_2\text{O}_3-400$  cal sample fully formed nanoparticles (>2 nm) are found to be selectively concentrated on unovercoated  $\text{Al}_2\text{O}_3$  nanospheres. Some subnanometer and 1 nm rafts are also observed over some discrete crystalline  $\text{ZnO}$  domains. Overall, this indicates significant Pt single-atom and small-domain stabilization by  $\text{ZnO}$  overcoating.

**CO Adsorption/DRIFTS Analysis.** Structural characterization of Pt center structures by CO chemisorption is an established method<sup>2,5,123–136</sup> for analyzing Pt species, including

single Pt atoms. Two C–O stretching modes having two different frequencies are commonly studied: that of CO adsorbed linearly to one Pt atom and that of CO adsorbed in a bridging fashion to two Pt atoms. Due to the breadth of the bridging peak, the linear CO stretch is more informative and allows probing of single atom and nanoparticle species. On the basis of literature reports, CO adsorbed on Pt nanoparticles has C–O stretching frequencies in the 2050–2100  $\text{cm}^{-1}$  range. Peaks at frequencies higher than 2100  $\text{cm}^{-1}$  are assigned to oxidized cationic Pt species, the chemical state in which single Pt atoms are known to exist.<sup>2,5,123–135</sup> For an illustration of linear CO binding modes and IR frequency band assignments, see Table 1. For  $(^{\text{Ph}}\text{PCP})\text{Pt-Al}_2\text{O}_3\text{-400 cal}$ , two peaks are

**Table 1. Illustration of CO Linearly Bound on Pt and Corresponding Spectroscopic Assignments**

CO bound to Pt NP's 2030 $\text{cm}^{-1}$ - 2120 $\text{cm}^{-1}$		
Frequency rises with oxidation state		
Bound CO reactive to $\text{O}_2$		
		
CO bound to Pt single atoms 2080 $\text{cm}^{-1}$ - 2115 $\text{cm}^{-1}$		
Bound CO less reactive to $\text{O}_2$ (except on $\text{CeO}_2$ and Fe oxide)		
		
Pt site	oxidation state	frequency ( $\text{cm}^{-1}$ )
nanoparticles	0	2030–2100
nanoparticles	cationic ( $2+$ or $\delta^+$ )	2080–2120
single atoms	cationic ( $2+$ or $\delta^+$ )	2080–2120

observed at 2118 and 2088  $\text{cm}^{-1}$ , both corresponding to linear C–O stretching modes (Figure 4). From literature precedent, the 2118  $\text{cm}^{-1}$  peak is assigned to CO adsorbed to single-atom Pt species, while that at 2088  $\text{cm}^{-1}$  is assigned to Pt nanoparticles. When the sample is heated to 100  $^\circ\text{C}$  under  $\text{O}_2$ , the peak at 2088  $\text{cm}^{-1}$  disappears, and the peak corresponding to CO adsorbed to single atoms remains. This result indicates that, at 100  $^\circ\text{C}$ , single-atom Pt on  $\text{Al}_2\text{O}_3$  is less capable of oxidizing CO, in accord with the conclusions of Moses-DeBusk et al.<sup>2</sup> In that study, the light-off temperature for CO oxidation over a Pt/ $\text{Al}_2\text{O}_3$  catalyst containing only single-atom Pt was reported to be 200  $^\circ\text{C}$ , whereas nanoparticle-containing catalysts mediated CO oxidation at far lower temperatures.<sup>2</sup> Also, recent work by Ding et al. shows that the single-atom Pt species on non-reducible oxides are not active sites for CO oxidation or the water-gas shift reaction.<sup>135</sup>

For the overcoated material 20Al- $(^{\text{Ph}}\text{PCP})\text{Pt-Al}_2\text{O}_3\text{-400 cal}$ , two peaks at 2110 and 2088  $\text{cm}^{-1}$  are similarly observed. These peaks are assigned analogously to those observed for  $(^{\text{Ph}}\text{PCP})\text{Pt-Al}_2\text{O}_3\text{-400 cal}$ . For this material, the ratio of the intensities between the peak assigned to single-atom Pt and the peak assigned to Pt nanoparticles is much greater. This result implies that the  $\text{Al}_2\text{O}_3$  overcoating significantly decreases the number of the exposed Pt nanoparticles by physically restricting access to these sites. Upon heating to 100  $^\circ\text{C}$  under  $\text{O}_2$  for 5 min, the single-atom peak remains, albeit slightly decreased in intensity, and the peak assigned to Pt nanoparticles is no longer observed.

For 40Ti- $(^{\text{Ph}}\text{PCP})\text{Pt-Al}_2\text{O}_3\text{-400 cal}$ , a peak at 2110  $\text{cm}^{-1}$  is observed and a smaller peak is observed at the region assigned

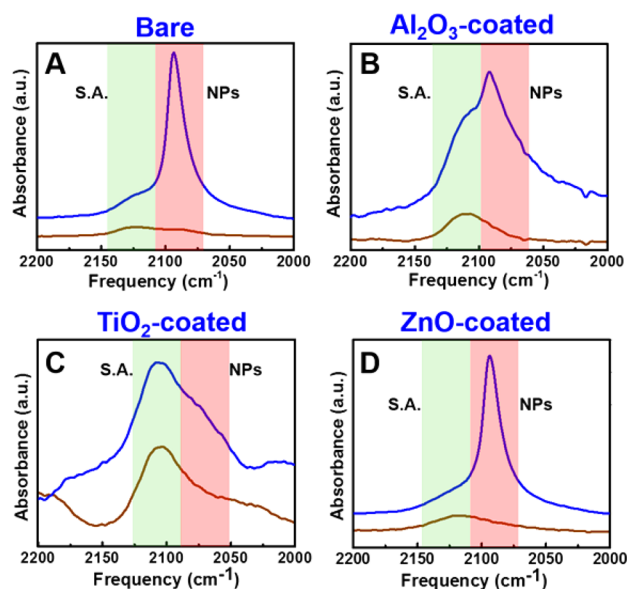


**Figure 4.** DRIFTS spectra (blue) of CO adsorbed on (A)  $(^{\text{Ph}}\text{PCP})\text{Pt-Al}_2\text{O}_3\text{-400 cal}$ , (B) 20Al- $(^{\text{Ph}}\text{PCP})\text{Pt-Al}_2\text{O}_3\text{-400 cal}$ , (C) 40Ti- $(^{\text{Ph}}\text{PCP})\text{Pt-Al}_2\text{O}_3\text{-400 cal}$ , (D) 20Zn- $(^{\text{Ph}}\text{PCP})\text{Pt-Al}_2\text{O}_3\text{-400 cal}$ , and accompanying spectra (brown) after desorption under  $\text{O}_2$  at 100  $^\circ\text{C}$ . Peak assignments for single atoms (S.A.) are in areas shaded in green and nanoparticles (NPs) in areas shaded in red.

to reduced Pt nanoparticles ( $<2100 \text{ cm}^{-1}$ ). The peak at 2110  $\text{cm}^{-1}$  is indicative of an oxidized Pt species on  $\text{TiO}_2$  and is thus assigned to the Pt single-atom species.<sup>137</sup> This is in agreement with the HAADF-STEM data, where very few Pt nanoparticles are observed. Upon heating in  $\text{O}_2$  to 100  $^\circ\text{C}$ , the peak at 2110  $\text{cm}^{-1}$  remains, while the shoulder at 2090  $\text{cm}^{-1}$  decreases in intensity. This indicates that highly oxidized single-atom species are less reactive than Pt nanoclusters for oxidizing adsorbed  $\text{CO}$ .<sup>2,135</sup>

The DRIFTS spectrum of CO adsorbed on 20Zn- $(^{\text{Ph}}\text{PCP})\text{Pt-Al}_2\text{O}_3$  also reveals a peak at 2090  $\text{cm}^{-1}$  and an overlapping peak at 2120  $\text{cm}^{-1}$  (Figure 4D). The lower frequency peak is assigned to reduced Pt nanoparticles. When the sample is heated to 100  $^\circ\text{C}$  under  $\text{O}_2$ , this peak vanishes while the higher frequency peak at 2120  $\text{cm}^{-1}$  remains, similarly to that of the  $\text{TiO}_2$ -coated sample.

**XPS Analysis.** Pt 4d<sub>5/2</sub> XPS studies were also performed on the supported Pt materials (Figure 5). Prior to calcination,  $(^{\text{Ph}}\text{PCP})\text{Pt-Al}_2\text{O}_3$  exhibits a spectral feature at approximately 316.0 eV. Because Pt 4d<sub>5/2</sub> binding energies due to Pt<sup>0</sup> species are commonly observed as high as 314.7 eV, this peak is assigned to the intact supported Pt<sup>2+</sup> organometallic. For bare calcined  $(^{\text{Ph}}\text{PCP})\text{Pt-Al}_2\text{O}_3\text{-400 cal}$ , features at 314.0 eV (70%) and 318.6 eV (30%) are observed and can be assigned to reduced Pt and oxidized Pt species, respectively.<sup>125,137–140</sup> On the basis of the intensity profiles, it is apparent that Pt<sup>0</sup> dominates on the bare material, indicating a preponderance of nanoparticle Pt species. For 20Al- $(^{\text{Ph}}\text{PCP})\text{Pt-Al}_2\text{O}_3\text{-400 cal}$ , peaks at 317.0 eV (42%) and 313.9 eV (58%) are apparent and similarly assigned.

The XPS spectrum of 40Ti- $(^{\text{Ph}}\text{PCP})\text{Pt-Al}_2\text{O}_3\text{-400 cal}$  exhibits a single feature at 316.3 eV, which is assigned to Pt<sup>2+</sup> complexes.<sup>137–140</sup> This implies that the material contains a large amount of oxidized species. Because both nanoparticles and single Pt atoms are observed by HAADF-STEM for this sample, it is reasonable to assign the feature to oxidized forms

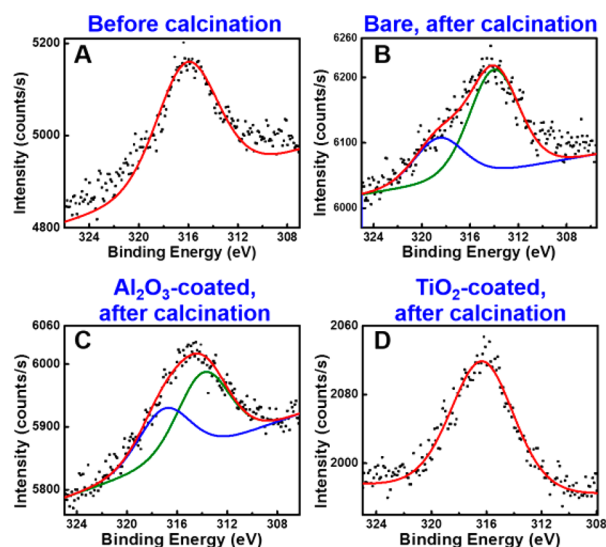


**Figure 5.** Pt  $4d_{3/2}$  XPS spectra of (A)  $(^{\text{Ph}}\text{PCP})\text{Pt}-\text{Al}_2\text{O}_3$ , (B)  $(^{\text{Ph}}\text{PCP})\text{Pt}-\text{Al}_2\text{O}_3-400$  cal, (C)  $20\text{Al}-(^{\text{Ph}}\text{PCP})\text{Pt}-\text{Al}_2\text{O}_3-400$  cal, and (D)  $40\text{Ti}-(^{\text{Ph}}\text{PCP})\text{Pt}-\text{Al}_2\text{O}_3-400$  cal: red, overall fit; green, reduced Pt fit; blue, oxidized Pt fit.

of both Pt species. The noticeably higher proportion of oxidized species is also consistent with the estimated percentage of single atoms in the  $\text{TiO}_2$ -overcoated sample (95%). XPS analysis of  $20\text{Zn}-(^{\text{Ph}}\text{PCP})\text{Pt}-\text{Al}_2\text{O}_3-400$  cal could not be acquired due to overlap with a Zn Auger peak.<sup>141</sup>

## DISCUSSION

The  $^{31}\text{P}$  NMR experiments performed in this study allow informative tracking of the state of the Pt precursor through the sequence of synthetic steps. First, by solution-phase NMR, we can confirm chemisorption of the intact  $(^{\text{Ph}}\text{PCP})\text{Pt}-\text{O}-$  entity on  $\text{Al}_2\text{O}_3$ . Known chemistries regarding similar Pd complexes,<sup>105</sup> and the fact that several washes with toluene do not leach the supported Pt species, argue that the deposition process is chemisorption and not physisorption. In either case, strong binding is confirmed by solid-state  $^{31}\text{P}$  NMR and ICP-AES analysis. In addition, the reactivity of the pincer complex on the surface is monitored by the solid-state  $^{31}\text{P}$  NMR experiments. Using this technique, it is found that the pincer complex retains its structural integrity throughout the ALD process. Thus, observing only phosphate species on the calcined materials by solid-state  $^{31}\text{P}$  NMR indicates that calcination under  $\text{O}_2$  at  $400^\circ\text{C}$  completely decomposes the pincer ligand. Furthermore, imaging of the precalcined material by AC-HAADF-STEM reveals no Pt nanoparticles. Both lines of evidence indicate that sintering takes place exclusively during calcination. Note that while surface dopants such as  $\text{Na}^{19,142}$  and  $\text{La}^3$  are known to stabilize Pt single atoms, surface phosphate species do not play a major role in the stabilization of Pt single atoms against sintering in the present system, as shown in the case of  $(^{\text{Ph}}\text{PCP})\text{Pt}-\text{Al}_2\text{O}_3-400$  cal. While it is likely that surface phosphates can potentially alter the electronics of Pt species, it is clear from the present results that sintering is inevitable unless an ALD overcoat is applied.

The synthetic strategy applied here selectively yields catalysts that predominantly contain single Pt atoms. For the bare/nonovercoated and the  $\text{Al}_2\text{O}_3$ -overcoated Pt centers, calcination at  $400^\circ\text{C}$  under  $\text{O}_2$  results in significant sintering, and particles up to 10 nm can be observed by AC-HAADF-STEM.  $\text{Al}_2\text{O}_3$ -

overcoated samples, however, exhibit significantly smaller average nanoparticle sizes relative to the bare sample (1.7 vs 3.8 nm). For Pt centers overcoated with  $\text{TiO}_2$  and  $\text{ZnO}$ , the largest Pt nanoparticles observed by AC-HAADF-STEM are ca. 2 and 5 nm, respectively. For the  $\text{TiO}_2$ -overcoated samples, an even greater single-atom Pt stabilization is observed and the area averaged estimates of the atom percentage of single-atom Pt support this assessment. Furthermore, although the area-density-based count of single atoms indicates that only ca. 41% of the Pt is in single-atom form in the  $\text{ZnO}$ -coated sample, it should be noted that only a small minority of the Pt nanoparticles 2 nm or greater (ca. 2% of the total imaged) are observed in areas where  $\text{ZnO}$  overcoats are clearly visible (10% of total area observed), implying that these overlayers are very effective for Pt single-atom stabilization. A similar study by Flytzani-Stephanopoulos et al. reported similar stabilization of Au single atoms and the inhibition of nanoparticle growth by  $\text{ZnO}$  domains on  $\text{ZrO}_2$ .<sup>8,11</sup> Note that the synthetic strategy employed here does not require the support to have a high surface area and can conceivably be applied to other oxides as well. Although our Pt loading is modest, in terms of surface metal density, the result ( $\sim 0.09$  Pt per  $\text{nm}^2$ ) is comparable to that of other oxide-supported Pt single-atom systems ( $0.01-0.16$  Pt/ $\text{nm}^2$ ).<sup>1,2,7,19,33,37</sup>

DRIFTS spectra of adsorbed CO reveal a similar trend. Thus, the bare Pt centers exhibit a much larger peak corresponding to Pt nanoparticles versus the overcoated Pt centers, although it should be noted that, because a significant portion of the Pt species are rendered physically inaccessible by the overcoats, qualitatively lower overall IR signal intensities are observed for the overcoated samples. The similarity in CO adsorption peak positions of the samples, bare and overcoated, suggests that the chemical environments of the exposed metal species are comparable. Furthermore, strong metal-support interactions (SMSI) between Pt and oxide layers such as  $\text{TiO}_2$  resulting in Pt encapsulation or migration into the overcoat is not likely, since reduction of the sample is a prerequisite for this to occur. Single Pt atoms supported on redox-active supports such as  $\text{FeO}_x$  and  $\text{TiO}_2$  are known to exhibit CO oxidation activity even at room temperature.<sup>1,142</sup> However, all samples in our study exhibit similar trends in CO oxidation experiments where CO adsorbed on single-atom Pt is more difficult to oxidize than CO adsorbed on Pt nanoparticles, even at  $100^\circ\text{C}$ . Our results are in agreement with the work of Moses-DeBusk et al.<sup>2</sup> and Ding et al.,<sup>135</sup> where Pt single atoms were exclusively supported on a non-redox-active oxide. Therefore, we believe that the Pt species we observe primarily reside on the support and possibly at the support-overcoat interface rather than migrating into the overcoat oxide layer.

Analysis of the XPS spectra of uncalcined  $(^{\text{Ph}}\text{PCP})\text{Pt}-\text{Al}_2\text{O}_3$  reveals a single feature at 316.0 eV, which supports the scenario that a discrete organometallic complex is adsorbed on the  $\text{Al}_2\text{O}_3$  support. After calcination, XPS of  $(^{\text{Ph}}\text{PCP})\text{Pt}-\text{Al}_2\text{O}_3-400$  cal and  $20\text{Al}-(^{\text{Ph}}\text{PCP})\text{Pt}-\text{Al}_2\text{O}_3-400$  cal indicates the presence of both reduced and oxidized Pt species. While the presence of  $\text{Pt}^0$  is undoubtedly an indication that nanoparticles are formed, the presence of  $\text{Pt}^{2+}$  or  $\text{Pt}^{4+}$  can be assigned to isolated single atoms, subnanometer clusters or interfacial sites, and nanoparticle surface sites. Thus, the exact proportions of  $\text{Pt}^{2+}$  and  $\text{Pt}^{4+}$  do not yield meaningful conclusions about the speciation of surface Pt and were not fitted explicitly. In contrast, the XPS spectrum of the  $\text{TiO}_2$ -overcoated  $40\text{Ti}-(^{\text{Ph}}\text{PCP})\text{Pt}-\text{Al}_2\text{O}_3-400$  cal sample shows exclusively oxidized Pt species. The presence

of the Pt<sup>0</sup> peak indicates Pt sintering and the formation of large Pt domains, while a symmetric Pt<sup>2+</sup> peak strongly suggests the presence of a single surface species. Note that, however, while the proportion of surface Pt<sup>2+</sup> seems to correlate with increased single-atom population, the correlation between XPS-derived oxidation states for surface Pt species and their coordination environment or thermal stability has not been unambiguously established. Although it is difficult to draw definitive conclusions regarding what exact oxidation state is more stable than the other, it is apparent that ALD overcoats in general increase the population of Pt single atoms and small Pt domains. For the bare and Al<sub>2</sub>O<sub>3</sub>-coated samples, these results corroborate the presence of a mixture of Pt nanoparticles and the divergence of the Pt XPS peak from Pt<sup>2+</sup> is an indication of increased heterogeneity of surface Pt species. On the basis of the DRIFTS and AC-HAADF-STEM data, the presence of only oxidized Pt species on the TiO<sub>2</sub>-overcoated sample is entirely consistent with the presence of a large percentage of single Pt atoms.

The percentage of accessible Pt sites was probed by measuring the quantity of CO adsorbed on the prepared materials. Thus, bare (<sup>Ph</sup>PCP)Pt-Al<sub>2</sub>O<sub>3</sub>-400 cal shows a dispersion of 26%, while 20Al-(<sup>Ph</sup>PCP)Pt-Al<sub>2</sub>O<sub>3</sub>-400 cal shows an even lower dispersion of 12%, which likely results from the Al<sub>2</sub>O<sub>3</sub> overcoats obstructing CO access to the Pt sites. Upon overcoating with TiO<sub>2</sub>, an increase in dispersion to 62% is observed, indicating the presence of far smaller Pt nuclearities. This high Pt surface accessibility can also be attributed to the fact that both TiO<sub>2</sub> crystallite formation and uniform overcoating are observed, which result, on average, in thinner overcoats (some of which are not easily observable by AC-HAADF-STEM). For the ZnO-coated samples, significant site blocking is observed, and only 26% of Pt sites are exposed, despite indications by HAADF-STEM that this material contains a large number of single Pt atoms and smaller nanoparticles. Apart from physical blocking by the ZnO overcoat, an alternative explanation that has been frequently advanced in the literature is Pt-Zn alloy formation, which is known to decrease CO uptake by Pt/ZnO catalysts.<sup>143</sup> Pt<sup>0</sup> and Zn<sup>0</sup> in close physical contact form intermetallic compounds at temperatures as low as 127 °C,<sup>144</sup> and H<sub>2</sub>-induced reduction and subsequent Pt-Zn alloy formation from Pt supported on ZnO can occur at 227 °C.<sup>145,146</sup> As discussed previously, sintering of surface Pt takes place exclusively during the calcination process; however, we further reduced the samples to show the effectiveness of the overcoats. As expected, CO adsorption measurements on 20Zn-(<sup>Ph</sup>PCP)Pt-Al<sub>2</sub>O<sub>3</sub>-400 cal reduced with H<sub>2</sub> at 250 °C indeed result in extensive adsorbed CO signal loss, indicative of alloy formation (Figure S8 in the Supporting Information). Similar CO adsorption measurements performed on other samples reduced in a similar fashion, however, give results similar (Figure S8) to those of the calcined samples: the CO adsorption peak assigned to CO adsorbed on Pt single atoms is more evident in the TiO<sub>2</sub>-overcoated sample, suggesting that TiO<sub>2</sub> overcoats are more effective at stabilizing Pt single atoms than Al<sub>2</sub>O<sub>3</sub> overcoats. While SMSI between Pt and TiO<sub>2</sub> can potentially play a role in the stabilization of the Pt single atoms, this nevertheless exemplifies the stabilization capacity of ALD-overcoated layers under conditions relevant to reactions such as the low-temperature water-gas shift<sup>22,135</sup> process. Such catalytic studies are beyond the scope of this paper, where we focus on the synthetic methodology of such potential catalysts.

The above data therefore suggest not only that the ALD overcoats increase the density of single Pt atoms and small Pt domains relative to larger Pt nanoparticles but also that they disproportionately reduce access to the Pt nanoparticles. Considering that sintering occurs despite the fact that the deposited monometallic Pt precursor is overcoated before it is calcined, it is likely that thermally induced migration of the Pt single atoms across the overcoats occurs. This is also a possible mechanism by which CO can gain access to overcoated single-atom Pt. While decreasing the number of ALD cycles may increase the quantity of accessible Pt, the relatively thick (1–2 nm) overcoats were deliberately selected to avoid significant “pinhole” densities present in thin TiO<sub>2</sub> and ZnO overcoats, especially at low temperature (50 °C). More importantly, selective sintering and agglomeration of Pt species were observed in the ZnO-coated sample, where the support was not fully coated. It is possible that sparse ZnO coverages (equivalent to a few ALD cycles) are present, but this cannot be rigorously confirmed by HAADF-STEM. While thinner ALD coatings may indeed provide stabilization of surface Pt, this is very difficult to prove, in contrast to the thicker coatings that can be readily verified by microscopy and other supporting data.

Finally, we note that the TiO<sub>2</sub> and ZnO overcoats are significantly more effective in stabilizing Pt single atoms and small Pt domains than are Al<sub>2</sub>O<sub>3</sub> overcoats. While the reason for this is currently not completely obvious, it is consistent with literature examples where heteroatom metal–oxo species dispersed onto oxide carriers are known to stabilize single noble metal atom species.<sup>3,8,11,19,21</sup> The stabilization of small Pt nanoparticles and single atoms by Al<sub>2</sub>O<sub>3</sub> overcoats may possibly arise from additional defect sites on the overcoat, since defect sites on Al<sub>2</sub>O<sub>3</sub> have previously been shown to stabilize single-atom Pt.<sup>2,37,38</sup>

## CONCLUSIONS

A novel rational synthetic methodology combining surface organometallic chemistry and overcoating by atomic layer deposition has been developed for the preparation of single-atom Pt catalysts on a commercially available Al<sub>2</sub>O<sub>3</sub> support with moderate surface area. It is shown that solution-phase grafting of the organometallic Pt precursor can atomically disperse the metal species on the support surface, while overcoating generally increases dispersion and increases the population of Pt single atoms even after harsh thermal treatment. In addition, TiO<sub>2</sub> overcoats stabilize smaller Pt species markedly more than Al<sub>2</sub>O<sub>3</sub> or ZnO overcoats, achieving >95% Pt single-atom population. This represents a widely applicable strategy of synthesizing supported single atoms without the need for high-surface-area supports and is potentially extendable to the synthesis of other supported single-atom catalyst systems with different organometallic precursor and oxide support combinations.

## EXPERIMENTAL SECTION

**General Considerations.** All manipulations of air- and moisture-sensitive compounds were carried out with rigorous exclusion of O<sub>2</sub> and moisture in flame- or oven-dried Schlenk-type glassware interfaced to a dual-manifold Schlenk line or a high-vacuum (10<sup>-5</sup>–10<sup>-6</sup> Torr) line or in an Ar filled MBraun Labstar glovebox with a high-capacity recirculator (<0.5 ppm of O<sub>2</sub>). All hydrocarbon solvents (*n*-pentane, benzene, and toluene) were purified using a Grubbs solvent system.<sup>147</sup> Diethyl ether and THF were distilled from Na/benzophenone ketyl.

All other starting materials were purchased from Sigma-Aldrich Chemical Co., Strem Chemicals Inc., or Alfa Aesar and used without further purification unless otherwise noted. The spherical  $\text{Al}_2\text{O}_3$  support (NanoArc, Alfa Aesar) used in this work is a 70:30 mixture of  $\delta$ - and  $\gamma$ -alumina, respectively, is nonporous, and has a surface area of 30–40  $\text{m}^2/\text{g}$ . All gases were purchased from Airgas or Matheson Tri-Gas. The complex  $(^{\text{Ph}}\text{PCP})\text{Pt-OH}^{103}$  was prepared by a modification of known literature methods (see the Supporting Information) and characterized by  $^1\text{H}$  and  $^{31}\text{P}$  NMR.

**Support Pretreatment.** Prior to any synthetic steps, the NanoArc  $\text{Al}_2\text{O}_3$  was pretreated by calcination for 4 h under  $\text{O}_2$  at 400  $^\circ\text{C}$  and then rehydroxylated overnight by flowing water vapor at 25  $^\circ\text{C}$ , delivered via a saturator. Finally, it was dried at 120  $^\circ\text{C}$  under high vacuum (ca.  $10^{-6}$  Torr) and then stored in an Ar-filled glovebox.

**Synthesis of Supported Organometallic Complex  $(^{\text{Ph}}\text{PCP})\text{Pt-Al}_2\text{O}_3$ .** In a typical procedure for the chemisorption of  $(^{\text{Ph}}\text{PCP})\text{Pt-OH}$  on  $\text{Al}_2\text{O}_3$ , 25 mg of the  $(^{\text{Ph}}\text{PCP})\text{Pt-OH}$  complex was loaded into a Schlenk flask. Separately, 6.0 g of NanoArc  $\text{Al}_2\text{O}_3$  was loaded into a flask, which was then attached onto a swivel-frit setup. The NanoArc  $\text{Al}_2\text{O}_3$  was slurried in 200 mL of toluene, after which a 100 mL toluene solution of  $(^{\text{Ph}}\text{PCP})\text{Pt-OH}$  was added via cannula filter dropwise into the  $\text{Al}_2\text{O}_3$  slurry with vigorous magnetic stirring. The sample was stirred overnight, the supernatant liquid removed via filtration, and the powder washed four times with 60 mL of toluene to remove any precursor that was not chemically bound to the  $\text{Al}_2\text{O}_3$  support. The resulting  $(^{\text{Ph}}\text{PCP})\text{Pt-Al}_2\text{O}_3$  powder was dried under vacuum overnight and stored in a glovebox. To measure the Pt content, samples were sent to Galbraith Laboratories for ICP-AES analysis. Samples used in this work were 0.09–0.1 wt % Pt unless otherwise stated.<sup>148</sup>

**ALD Overcoating of  $(^{\text{Ph}}\text{PCP})\text{Pt-Al}_2\text{O}_3$ .** All ALD overcoating processes were performed in a home-built viscous flow reactor.<sup>149</sup> The reactor was maintained at a pressure of 1–2 Torr and was under constant ultrahigh-purity  $\text{N}_2$  flow at 200 sccm for the duration of the ALD processes.  $\text{Al}(\text{CH}_3)_3$  (TMA) and deionized water were used to grow  $\text{Al}_2\text{O}_3$  layers,  $\text{Zn}(\text{C}_2\text{H}_5)_2$  and deionized water were used to grow ZnO layers, and  $\text{Ti}[\text{N}(\text{CH}_3)_2]_4$  (TDMAT) and deionized water were used to grow  $\text{TiO}_2$  overcoats. To obtain sufficient vapor pressure and growth, the TDMAT precursor was dosed from a stainless steel saturator at room temperature. All films were grown at a reactor temperature of 50  $^\circ\text{C}$ . Mass gains were quantified by weighing the sample tray before and after the overcoating process.

Timing sequences for the ALD cycles are expressed in the form  $t_1$ – $t_2$ – $t_3$ – $t_4$ , where  $t_1$  is the duration of the “A” precursor,  $t_2$  is the duration (in s) of the corresponding purge,  $t_3$  is the duration of the “B” precursor, and  $t_4$  is then the duration of its corresponding purge. For TMA/ $\text{H}_2\text{O}$ , 1.0 g of substrate was loaded onto the reactor and a timing sequence of 600–600–600–600 was used. For  $\text{Zn}(\text{C}_2\text{H}_5)_2/\text{H}_2\text{O}$ , 0.5 g of substrate was loaded into the reactor and a corresponding timing sequence of 300–600–300–600 was used. For TDMAT/ $\text{H}_2\text{O}$ , 0.5 g of substrate was loaded into the reactor and a timing sequence of 150–450–150–450 was used.

**Calcination.** To remove the remaining ligands and organics and obtain the final activated material, both uncoated and overcoated samples were calcined in a Lindberg/Blue-M TF55035A tube furnace at 400  $^\circ\text{C}$  (unless otherwise stated) under flowing  $\text{O}_2$  for 4 h. Henceforth, the materials nomenclature will specify the number of oxide ALD overcoating cycles, the material, and the calcination temperature under  $\text{O}_2$  in  $^\circ\text{C}$ .

**Solid-State  $^{31}\text{P}$  NMR.**  $^{31}\text{P}$  cross-polarization magic angle spinning (CPMAS) solid-state NMR spectra were recorded on a Varian VXR400 spectrometer, equipped with a 5 mm triple-resonance probe operated at a MAS rate of 10 kHz. Samples were loaded into cylindrical zirconia rotors and capped with a solid Teflon cap (in a glovebox if uncalcined). For routine CPMAS  $^{31}\text{P}$  spectra, the following sequence was used: (i) 90 $^\circ$  pulse at the proton frequency (pulse width 3.4 s), (ii) cross-polarization step with a contact time of 5 ms, and (iii) acquisition of the  $^{31}\text{P}$  signal under high-power (50 W) proton decoupling with a recycle delay time of 5 s, to allow the complete relaxation of the  $^1\text{H}$  nuclei. Peaks were referenced to  $\text{NH}_4\text{H}_2\text{PO}_4$ , which is known to have a chemical shift of 0.8 ppm with respect to

85%  $\text{H}_3\text{PO}_4$ .<sup>150</sup> Approximately 5000–10000 scans were needed to obtain a satisfactory signal.

**CO Adsorption/Diffuse Reflectance Infrared Spectroscopy (DRIFTS).** DRIFTS spectra were obtained on a Nicolet 6700 FT-IR spectrometer, located at the Northwestern University CleanCat Facility, with a resolution of 4  $\text{cm}^{-1}$ . Samples were held in a Harrick Praying Mantis cell equipped with either KBr or ZnSe windows. The cell was equipped with a gas inlet and vent to allow the feeding of desired reactant or pretreatment gases. In a typical experiment, the sample was pretreated under zero grade air at 150  $^\circ\text{C}$  for 1 h and cooled to room temperature and the background was allowed to stabilize for 1–2 h. The stability of the background was evaluated by taking a background spectrum and then subsequently taking spectra with this background subtracted. Afterward, the system was placed under Ar for 5–10 min and a background spectrum was undertaken, after which 1% CO in  $\text{N}_2$  was dosed into the cell until no further growth of peaks corresponding to chemisorbed CO were observed. Any remaining CO was then purged out with argon gas for 5 min, at which point infrared bands due to free CO were no longer observable. Then spectra of the material with adsorbed CO were obtained.

**Aberration Corrected High Angle Annular Dark Field Transmission Electron Microscopy (AC-HAADF-STEM).** Images were obtained on a JEOL JEMARM200CF electron microscope operating at 200 kV for high spatial resolution HAADF imaging with an inner collecting angle of 68 mrad and outer collecting angle of 230 mrad. A probe side Cs corrector was used to create a probe size of approximately 0.078 nm. Under daily operating conditions, the third-order aberrations remain stable for days while the second-order aberrations were monitored and corrected as needed during the experiments. In this mode, species with higher atomic weight appear brighter than those with lower atomic weight. The samples were either loaded as dry powder specimens or drop-cast as a suspension in ethanol onto a Cu grid with a carbon film support. Images were processed and rendered using Gatan Digital Micrograph software. Particles and single atoms were manually counted, and particle diameters were measured manually using ImageJ.<sup>151</sup> For all of the calcined samples, 200–500 domains, including single atoms, subnanometer clusters, and fully formed nanoparticles were observed. In some images, occasional Pt “dimers” were observed. These were counted as separate single atoms, because it could not be ascertained whether these species form as a consequence of single-atom movement induced by electron beam exposure.

**X-ray Photoelectron Spectroscopy.** XPS spectra were collected on a Thermo Scientific ESCALAB 250Xi instrument, equipped with an Al K $\alpha$  radiation source, in a pressure of  $10^{-7}$  mbar at a pass energy of 50 eV. Because XPS peaks from the Al 2p electrons overlap with the Pt 4f $_{7/2}$  line, which is the most intense of the Pt lines, binding energies from the Pt 4d $_{5/2}$  electrons were investigated instead. Binding energies were referenced against that of adventitious carbon, which was set at 284.8 eV. Typically, a 100 ms dwell time and 100–200 scans were used for each spectrum. Spectra were corrected using a Shirley type background correction. Peaks were fitted with full widths at half-maximum of 4–6 eV.

**Dispersion Measurements.** Access to Pt sites was determined by CO pulse chemisorption<sup>152,153</sup> on an AMI-200 TPR/TPO gas sorption instrument with a TCD detector, located at the Northwestern University CleanCat Facility. Prior to CO dosing, a sample of known mass and Pt loading was prerduced at 150  $^\circ\text{C}$  under  $\text{H}_2$ . Then, a known volume of 1% CO/He was dosed at 40  $^\circ\text{C}$ . Any CO not strongly bound to the sample was then purged into the TCD detector. The pulsing and purging process was repeated 30 times. The signal detected for the last five pulses, during which time adsorption no longer occurred, was used as the baseline for zero adsorption. Assuming a 1:1 CO:Pt ratio, the number of accessible Pt sites was calculated as the number of moles of CO adsorbed divided by the total number of moles of Pt, as measured by ICP analysis. For ALD-overcoated samples, the number of moles of Pt was obtained by using the Pt weight loading of the un-overcoated material and appropriately adjusting it, taking into account the measured mass gain from the ALD process. This protocol was also tested against a Pt/ $\text{Al}_2\text{O}_3$  standard with



34% dispersion provided by Altamira Corp. and was found to be accurate to within  $\pm 10\%$ .

## ■ ASSOCIATED CONTENT

### Supporting Information

The Supporting Information is available free of charge on the ACS Publications website at DOI: 10.1021/acs.organomet.6b00869.

<sup>1</sup>H NMR, solid-state <sup>31</sup>P CPMAS NMR, additional electron microscopy images, and DRIFTS procedure for reduced samples (PDF)

## ■ AUTHOR INFORMATION

### Corresponding Authors

\*E-mail for T.J.M.: t-marks@northwestern.edu.

\*E-mail for P.C.S.: pstair@northwestern.edu.

### ORCID

Lawrence A. Crosby: 0000-0001-7644-3762

Massimiliano Delferro: 0000-0002-4443-165X

Tobin J. Marks: 0000-0001-8771-0141

### Present Address

#Chemical Sciences and Engineering Division, Argonne National Laboratory, Lemont, Illinois 60439, United States.

### Author Contributions

<sup>†</sup>These authors contributed equally.

### Notes

The authors declare no competing financial interest.

## ■ ACKNOWLEDGMENTS

This research is based upon work supported by the U.S. Department of Energy, Office of Science, Office of Basic Energy Sciences, under Award Number DOE DE-FG02-03ER154757. This work made use of the (EPIC, Keck-II) facilities of the NUANCE Center at Northwestern University, which has received support from the Soft and Hybrid Nanotechnology Experimental (SHyNE) Resource (NSF NNCI-1542205), the MRSEC program (NSF DMR-1121262) at the Materials Research Center, the International Institute for Nanotechnology (IIN), the Keck Foundation, and the State of Illinois, through the IIN. This work also made use of instruments at the IMSERC center at Northwestern University which were supported by the National Science Foundation under NSF CHE-9871268 (1998) and NSF CHE-1048773 and NSF DMR-0521267 (2005). The CleanCat Core facility acknowledges funding from the Department of Energy (DE-FG02-03ER15457 and DE-AC02-06CH11357) used for the purchase of the Nicolet 6700 FT-IR, Harrick DRIFTS accessory, and Altamira AMI-200.

## ■ REFERENCES

- (1) Qiao, B.; Wang, A.; Yang, X.; Allard, L. F.; Jiang, Z.; Cui, Y.; Liu, J.; Li, J.; Zhang, T. *Nat. Chem.* **2011**, *3*, 634–641.
- (2) Moses-DeBusk, M.; Yoon, M.; Allard, L. F.; Mullins, D. R.; Wu, Z.; Yang, X.; Veith, G.; Stocks, G. M.; Narula, C. K. *J. Am. Chem. Soc.* **2013**, *135*, 12634–12645.
- (3) Peterson, E. J.; DeLaRiva, A. T.; Lin, S.; Johnson, R. S.; Guo, H.; Miller, J. T.; Hun Kwak, J.; Peden, C. H. F.; Kiefer, B.; Allard, L. F.; Ribeiro, F. H.; Datye, A. K. *Nat. Commun.* **2014**, *5*, 4885.
- (4) Qiao, B.; Liu, J.; Wang, Y.-G.; Lin, Q.; Liu, X.; Wang, A.; Li, J.; Zhang, T.; Liu, J. *ACS Catal.* **2015**, *5*, 6249–6254.

- (5) Kistler, J. D.; Chotigkrai, N.; Xu, P.; Enderle, B.; Praserthdam, P.; Chen, C.-Y.; Browning, N. D.; Gates, B. C. *Angew. Chem., Int. Ed.* **2014**, *53*, 8904–8907.
- (6) Jones, J.; Xiong, H.; DeLaRiva, A. T.; Peterson, E. J.; Pham, H.; Challa, S. R.; Qi, G.; Oh, S.; Wiebenga, M. H.; Pereira Hernández, X. I.; Wang, Y.; Datye, A. K. *Science* **2016**, *353*, 150–154.
- (7) Gu, X.-K.; Qiao, B.; Huang, C.-Q.; Ding, W.-C.; Sun, K.; Zhan, E.; Zhang, T.; Liu, J.; Li, W.-X. *ACS Catal.* **2014**, *4*, 3886–3890.
- (8) Wang, C.; Boucher, M.; Yang, M.; Saltsburg, H.; Flytzani-Stephanopoulos, M. *Applied Catalysis B: Appl. Catal., B* **2014**, *154–155*, 142–152.
- (9) Yi, N.; Si, R.; Saltsburg, H.; Flytzani-Stephanopoulos, M. *Energy Environ. Sci.* **2010**, *3*, 831–837.
- (10) Hackett, S. F. J.; Brydson, R. M.; Gass, M. H.; Harvey, I.; Newman, A. D.; Wilson, K.; Lee, A. F. *Angew. Chem., Int. Ed.* **2007**, *46*, 8593–8596.
- (11) Wang, C.; Garbarino, G.; Allard, L. F.; Wilson, F.; Busca, G.; Flytzani-Stephanopoulos, M. *ACS Catal.* **2016**, *6*, 210–218.
- (12) Vilé, G.; Albani, D.; Nachtegaal, M.; Chen, Z.; Dontsova, D.; Antonietti, M.; López, N.; Pérez-Ramírez, J. *Angew. Chem., Int. Ed.* **2015**, *54*, 11265–11269.
- (13) Yan, H.; Cheng, H.; Yi, H.; Lin, Y.; Yao, T.; Wang, C.; Li, J.; Wei, S.; Lu, J. *J. Am. Chem. Soc.* **2015**, *137*, 10484–10487.
- (14) Corma, A.; Salnikow, O. G.; Barskiy, D. A.; Kovtunov, K. V.; Koptuyg, I. V. *Chem. - Eur. J.* **2015**, *21*, 7012–7015.
- (15) Pei, G. X.; Liu, X. Y.; Wang, A.; Lee, A. F.; Isaacs, M. A.; Li, L.; Pan, X.; Yang, X.; Wang, X.; Tai, Z.; Wilson, K.; Zhang, T. *ACS Catal.* **2015**, *5*, 3717–3725.
- (16) Zhang, L.; Wang, A.; Miller, J. T.; Liu, X.; Yang, X.; Wang, W.; Li, L.; Huang, Y.; Mou, C.-Y.; Zhang, T. *ACS Catal.* **2014**, *4*, 1546–1553.
- (17) Lin, J.; Wang, A.; Qiao, B.; Liu, X.; Yang, X.; Wang, X.; Liang, J.; Li, J.; Liu, J.; Zhang, T. *J. Am. Chem. Soc.* **2013**, *135*, 15314–15317.
- (18) Yang, M.; Allard, L. F.; Flytzani-Stephanopoulos, M. *J. Am. Chem. Soc.* **2013**, *135*, 3768–3771.
- (19) Yang, M.; Liu, J.; Lee, S.; Zugic, B.; Huang, J.; Allard, L. F.; Flytzani-Stephanopoulos, M. *J. Am. Chem. Soc.* **2015**, *137*, 3470–3473.
- (20) Fu, Q.; Saltsburg, H.; Flytzani-Stephanopoulos, M. *Science* **2003**, *301*, 935–938.
- (21) Yang, M.; Li, S.; Wang, Y.; Herron, J. A.; Xu, Y.; Allard, L. F.; Lee, S.; Huang, J.; Mavrikakis, M.; Flytzani-Stephanopoulos, M. *Science* **2014**, *346*, 1498–1501.
- (22) Zhai, Y.; Pierre, D.; Si, R.; Deng, W.; Ferrin, P.; Nilekar, A. U.; Peng, G.; Herron, J. A.; Bell, D. C.; Saltsburg, H.; Mavrikakis, M.; Flytzani-Stephanopoulos, M. *Science* **2010**, *329*, 1633–1636.
- (23) Flytzani-Stephanopoulos, M. *Acc. Chem. Res.* **2014**, *47*, 783–792.
- (24) Deng, W.; Flytzani-Stephanopoulos, M. *Angew. Chem., Int. Ed.* **2006**, *45*, 2285–2289.
- (25) Deng, W.; Frenkel, A. I.; Si, R.; Flytzani-Stephanopoulos, M. *J. Phys. Chem. C* **2008**, *112*, 12834–12840.
- (26) Deng, W.; Carpenter, C.; Yi, N.; Flytzani-Stephanopoulos, M. *Top. Catal.* **2007**, *44*, 199–208.
- (27) Si, R.; Flytzani-Stephanopoulos, M. *Angew. Chem., Int. Ed.* **2008**, *47*, 2884–2887.
- (28) Pierre, D.; Deng, W.; Flytzani-Stephanopoulos, M. *Top. Catal.* **2007**, *46*, 363–373.
- (29) Qiao, B.; Liang, J.-X.; Wang, A.; Xu, C.-Q.; Li, J.; Zhang, T.; Liu, J. *Nano Res.* **2015**, *8*, 2913–2924.
- (30) Lin, J.; Qiao, B.; Li, N.; Li, L.; Sun, X.; Liu, J.; Wang, X.; Zhang, T. *Chem. Commun.* **2015**, *51*, 7911–7914.
- (31) Chen, Y.; Kasama, T.; Huang, Z.; Hu, P.; Chen, J.; Liu, X.; Tang, X. *Chem. - Eur. J.* **2015**, *21*, 17397–17402.
- (32) Wei, H.; Liu, X.; Wang, A.; Zhang, L.; Qiao, B.; Yang, X.; Huang, Y.; Miao, S.; Liu, J.; Zhang, T. *Nat. Commun.* **2014**, *5*, 5634.
- (33) Nguyen, L.; Zhang, S.; Wang, L.; Li, Y.; Yoshida, H.; Patlolla, A.; Takeda, S.; Frenkel, A. I.; Tao, F. *ACS Catal.* **2016**, *6*, 840–850.
- (34) Shin, H. H.; Lu, L.; Yang, Z.; Kiely, C. J.; McIntosh, S. *ACS Catal.* **2016**, *6*, 2811–2818.

- (35) Choi, C. H.; Kim, M.; Kwon, H. C.; Cho, S. J.; Yun, S.; Kim, H.-T.; Mayrhofer, K. J. J.; Kim, H.; Choi, M. *Nat. Commun.* **2016**, *7*, 10922.
- (36) Yang, X.-F.; Wang, A.; Qiao, B.; Li, J.; Liu, J.; Zhang, T. *Acc. Chem. Res.* **2013**, *46*, 1740–1748.
- (37) Kwak, J. H.; Hu, J.; Mei, D.; Yi, C.-W.; Kim, D. H.; Peden, C. H. F.; Allard, L. F.; Szanyi, J. *Science* **2009**, *325*, 1670–1673.
- (38) Mei, D.; Kwak, J. H.; Hu, J.; Cho, S. J.; Szanyi, J.; Allard, L. F.; Peden, C. H. F. *J. Phys. Chem. Lett.* **2010**, *1*, 2688–2691.
- (39) Zugic, B.; Zhang, S.; Bell, D. C.; Tao, F.; Flytzani-Stephanopoulos, M. *J. Am. Chem. Soc.* **2014**, *136*, 3238–3245.
- (40) Fu, Q.; Deng, W.; Saltsburg, H.; Flytzani-Stephanopoulos, M. *Appl. Catal., B* **2005**, *56*, 57–68.
- (41) Yang, S.; Kim, J.; Tak, Y. J.; Soon, A.; Lee, H. *Angew. Chem., Int. Ed.* **2016**, *55*, 2058–2062.
- (42) Johnson, G. E.; Hu, Q.; Laskin, J. *Annu. Rev. Anal. Chem.* **2011**, *4*, 83–104.
- (43) Abbet, S.; Judai, K.; Klinger, L.; Heiz, U. *Pure Appl. Chem.* **2002**, *74*, 1527–1535.
- (44) Abbet, S.; Sanchez, A.; Heiz, U.; Schneider, W. D.; Ferrari, A. M.; Pacchioni, G.; Rösch, N. *J. Am. Chem. Soc.* **2000**, *122*, 3453–3457.
- (45) Choi, Y. S.; Moschetta, E. G.; Miller, J. T.; Fasulo, M.; McMurdo, M. J.; Rioux, R. M.; Tilley, T. D. *ACS Catal.* **2011**, *1*, 1166–1177.
- (46) Ruddy, D. A.; Jarupatrakorn, J.; Rioux, R. M.; Miller, J. T.; McMurdo, M. J.; McBee, J. L.; Tupper, K. A.; Tilley, T. D. *Chem. Mater.* **2008**, *20*, 6517–6527.
- (47) Baudouin, D.; Candy, J.-P.; Rodemerck, U.; Krumeich, F.; Veyre, L.; Webb, P. B.; Thieuleux, C.; Copéret, C. *Catal. Today* **2014**, *235*, 237–244.
- (48) Conley, M.; Copéret, C. *Top. Catal.* **2014**, *57*, 843–851.
- (49) Conley, M. P.; Copéret, C.; Thieuleux, C. *ACS Catal.* **2014**, *4*, 1458–1469.
- (50) Grüning, W. R.; Siddiqi, G.; Safonova, O. V.; Copéret, C. *Adv. Synth. Catal.* **2014**, *356*, 673–679.
- (51) Héroguel, F.; Gebert, D.; Detwiler, M. D.; Zemlyanov, D. Y.; Baudouin, D.; Copéret, C. *J. Catal.* **2014**, *316*, 260–269.
- (52) Héroguel, F.; Siddiqi, G.; Detwiler, M. D.; Zemlyanov, D. Y.; Safonova, O. V.; Copéret, C. *J. Catal.* **2015**, *321*, 81–89.
- (53) Oakton, E.; Vile, G.; Levine, D.; Zocher, E.; Baudouin, D.; Perez-Ramirez, J.; Coperet, C. *Dalton Trans.* **2014**, *43*, 15138–15142.
- (54) Siddiqi, G.; Mougél, V.; Coperet, C. *Dalton Trans.* **2015**, *44*, 14349–14353.
- (55) Serna, P.; Gates, B. C. *Acc. Chem. Res.* **2014**, *47*, 2612–2620.
- (56) Khivantsev, K.; Vityuk, A.; Aleksandrov, H. A.; Vayssilov, G. N.; Alexeev, O. S.; Amiridis, M. D. *J. Phys. Chem. C* **2015**, *119*, 17166–17181.
- (57) Martinez-Macias, C.; Chen, M.; Dixon, D. A.; Gates, B. C. *Chem. - Eur. J.* **2015**, *21*, 11825–11835.
- (58) Martinez-Macias, C.; Serna, P.; Gates, B. C. *ACS Catal.* **2015**, *5*, 5647–5656.
- (59) Bonati, M. L. M.; Douglas, T. M.; Gaemers, S.; Guo, N. *Organometallics* **2012**, *31*, 5243–5251.
- (60) Rimoldi, M.; Mezzetti, A. *Catal. Sci. Technol.* **2014**, *4*, 2724–2740.
- (61) Wegener, S. L.; Marks, T. J.; Stair, P. C. *Acc. Chem. Res.* **2012**, *45*, 206–214.
- (62) Williams, L. A.; Marks, T. J. *ACS Catal.* **2011**, *1*, 238–245.
- (63) Wegener, S. L.; Kim, H.; Marks, T. J.; Stair, P. C. *J. Phys. Chem. Lett.* **2011**, *2*, 170–175.
- (64) Williams, L. A.; Marks, T. J. *Organometallics* **2009**, *28*, 2053–2061.
- (65) Nicholas, C. P.; Marks, T. J. *Nano Lett.* **2004**, *4*, 1557–1559.
- (66) Nicholas, C. P.; Marks, T. J. *Langmuir* **2004**, *20*, 9456–9462.
- (67) Nicholas, C. P.; Ahn, H.; Marks, T. J. *J. Am. Chem. Soc.* **2003**, *125*, 4325–4331.
- (68) Ahn, H.; Nicholas, C. P.; Marks, T. J. *Organometallics* **2002**, *21*, 1788–1806.
- (69) Ahn, H.; Marks, T. J. *J. Am. Chem. Soc.* **2002**, *124*, 7103–7110.
- (70) Stalzer, M. M.; Delferro, M.; Marks, T. J. *Catal. Lett.* **2015**, *145*, 3–14.
- (71) Gu, W.; Stalzer, M. M.; Nicholas, C. P.; Bhattacharyya, A.; Motta, A.; Gallagher, J. R.; Zhang, G.; Miller, J. T.; Kobayashi, T.; Pruski, M.; Delferro, M.; Marks, T. J. *J. Am. Chem. Soc.* **2015**, *137*, 6770–6780.
- (72) Copéret, C.; Comas-Vives, A.; Conley, M. P.; Estes, D. P.; Fedorov, A.; Mougél, V.; Nagae, H.; Núñez-Zarur, F.; Zhizhko, P. A. *Chem. Rev.* **2016**, *116*, 323–421.
- (73) Richmond, M. K.; Scott, S. L.; Yap, G. P. A.; Alper, H. *Organometallics* **2002**, *21*, 3395–3400.
- (74) Yang, D.; Xu, P.; Guan, E.; Browning, N. D.; Gates, B. C. *J. Catal.* **2016**, *338*, 12–20.
- (75) Rubio-Marqués, P.; Rivero-Crespo, M. A.; Leyva-Pérez, A.; Corma, A. *J. Am. Chem. Soc.* **2015**, *137*, 11832–11837.
- (76) Villaverde, G.; Corma, A.; Iglesias, M.; Sanchez, F. *ACS Catal.* **2012**, *2*, 399–406.
- (77) Villaverde, G.; Corma, A.; Iglesias, M.; Sanchez, F. *ChemCatChem* **2011**, *3*, 1320–1328.
- (78) del Pozo, C.; Corma, A.; Iglesias, M.; Sanchez, F. *Organometallics* **2010**, *29*, 4491–4498.
- (79) Corma, A.; Gonzalez-Arellano, C.; Iglesias, M.; Sanchez, F. *Appl. Catal., A* **2010**, *375*, 49–54.
- (80) del Pozo, C.; Debono, N.; Corma, A.; Iglesias, M.; Sanchez, F. *ChemSusChem* **2009**, *2*, 650–657.
- (81) Fu, B.; Lu, J.; Stair, P. C.; Xiao, G.; Kung, M. C.; Kung, H. H. *J. Catal.* **2013**, *297*, 289–295.
- (82) Lu, J.; Fu, B.; Kung, M. C.; Xiao, G.; Elam, J. W.; Kung, H. H.; Stair, P. C. *Science* **2012**, *335*, 1205–1208.
- (83) Feng, H.; Lu, J.; Stair, P.; Elam, J. *Catal. Lett.* **2011**, *141*, 512–517.
- (84) Puurunen, R. L. *J. Appl. Phys.* **2005**, *97*, 121301–121301–121352.
- (85) Puurunen, R. L.; Lindblad, M.; Root, A.; Krause, A. O. I. *Phys. Chem. Chem. Phys.* **2001**, *3*, 1093–1102.
- (86) Yamada, A.; Sang, B.; Konagai, M. *Appl. Surf. Sci.* **1997**, *112*, 216–222.
- (87) Yousfi, E. B.; Fouache, J.; Lincot, D. *Appl. Surf. Sci.* **2000**, *153*, 223–234.
- (88) Lim, J. W.; Yun, S. J.; Lee, J. H. *Electrochem. Solid-State Lett.* **2004**, *7*, F73–F76.
- (89) Xie, Q.; Jiang, Y.-L.; Detavernier, C.; Deduytsche, D.; Van Meirhaeghe, R. L.; Ru, G.-P.; Li, B.-Z.; Qu, X.-P. *J. Appl. Phys.* **2007**, *102*, 083521.
- (90) George, S. M. *Chem. Rev.* **2010**, *110*, 111–131.
- (91) Bian, S.-W.; Liu, S.; Guo, M.-X.; Xu, L.-L.; Chang, L. *RSC Adv.* **2015**, *5*, 11913–11916.
- (92) Bo, Z.; Eaton, T. R.; Gallagher, J. R.; Canlas, C. P.; Miller, J. T.; Notestein, J. M. *Chem. Mater.* **2015**, *27*, 1269–1277.
- (93) Cheng, N.; Banis, M. N.; Liu, J.; Riese, A.; Li, X.; Li, R.; Ye, S.; Knights, S.; Sun, X. *Adv. Mater. (Weinheim, Ger.)* **2015**, *27*, 277–281.
- (94) Takenaka, S.; Miyazaki, T.; Matsune, H.; Kishida, M. *Catal. Sci. Technol.* **2015**, *5*, 1133–1142.
- (95) Wan, C.; Cheng, D.-g.; Chen, F.; Zhan, X. *Chem. Commun.* **2015**, *51*, 9785–9788.
- (96) Zhang, C.; Zhou, Y.; Zhang, Y.; Wang, Q.; Xu, Y. *RSC Adv.* **2015**, *5*, 12472–12479.
- (97) Zhang, C.; Zhou, Y.; Zhang, Y.; Zhang, Z.; Xu, Y.; Wang, Q. *RSC Adv.* **2015**, *5*, 64951–64960.
- (98) Zhang, Z.-c.; Xu, B.; Wang, X. *Chem. Soc. Rev.* **2014**, *43*, 7870–7886.
- (99) Lu, P.; Campbell, C. T.; Xia, Y. *Nano Lett.* **2013**, *13*, 4957–4962.
- (100) Min, B. K.; Wallace, W. T.; Goodman, D. W. *J. Phys. Chem. B* **2004**, *108*, 14609–14615.
- (101) Dai, Y.; Lim, B.; Yang, Y.; Cogley, C. M.; Li, W.; Cho, E. C.; Grayson, B.; Fanson, P. T.; Campbell, C. T.; Sun, Y.; Xia, Y. *Angew. Chem., Int. Ed.* **2010**, *49*, 8165–8168.

- (102) Liu, S.; Tan, J. M.; Gulec, A.; Schweitzer, N. M.; Delferro, M.; Marks, L. D.; Stair, P. C.; Marks, T. J. *ACS Catal.* **2016**, *6*, 8380–8388.
- (103) Bennett, M. A.; Jin, H.; Willis, A. C. *J. Organomet. Chem.* **1993**, *451*, 249–256.
- (104) Arunachalampillai, A.; Loganathan, N.; Wendt, O. F. *Polyhedron* **2012**, *32*, 24–29.
- (105) Fulmer, G. R.; Herndon, A. N.; Kaminsky, W.; Kemp, R. A.; Goldberg, K. I. *J. Am. Chem. Soc.* **2011**, *133*, 17713–17726.
- (106) Fulmer, G. R.; Muller, R. P.; Kemp, R. A.; Goldberg, K. I. *J. Am. Chem. Soc.* **2009**, *131*, 1346–1347.
- (107) Richmond, M. K.; Scott, S. L.; Alper, H. *J. Am. Chem. Soc.* **2001**, *123*, 10521–10525.
- (108) Kroto, H. W.; Klein, S. L.; Meidine, M. F.; Nixon, J. F.; Harris, R. K.; Packer, K. J.; Reams, P. J. *Organomet. Chem.* **1985**, *280*, 281–287.
- (109) Power, W. P.; Wasylishen, R. E. *Inorg. Chem.* **1992**, *31*, 2176–2183.
- (110) Mastrorilli, P.; Todisco, S.; Bagno, A.; Gallo, V.; Latronico, M.; Fortuño, C.; Gudat, D. *Inorg. Chem.* **2015**, *54*, 5855–5863.
- (111) Bleam, W.; Pfeffer, P.; Frye, J. *Phys. Chem. Miner.* **1989**, *16*, 455–464.
- (112) Decanio, E. C.; Edwards, J. C.; Scalzo, T. R.; Storm, D. A.; Bruno, J. W. *J. Catal.* **1991**, *132*, 498–511.
- (113) Georgelin, T.; Jaber, M.; Onfroy, T.; Hargrove, A.-A.; Costa-Torro, F.; Lambert, J.-F. *J. Phys. Chem. C* **2013**, *117*, 12579–12590.
- (114) Uzun, A.; Ortalan, V.; Browning, N. D.; Gates, B. C. *J. Catal.* **2010**, *269*, 318–328.
- (115) Uzun, A.; Ortalan, V.; Hao, Y.; Browning, N. D.; Gates, B. C. *J. Phys. Chem. C* **2009**, *113*, 16847–16849.
- (116) Song, K.; Sauter, D. J.; Wu, J.; Dravid, V. P.; Stair, P. C. *ACS Catal.* **2012**, *2*, 384–390.
- (117) Isaacson, M. S.; Langmore, J.; Parker, N. W.; Kopf, D.; Utlaut, M. *Ultramicroscopy* **1976**, *1*, 359–376.
- (118) Isaacson, M.; Kopf, D.; Utlaut, M.; Parker, N. W.; Crewe, A. V. *Proc. Natl. Acad. Sci. U. S. A.* **1977**, *74*, 1802–1806.
- (119) Bradley, S.; Sinkler, W.; Blom, D.; Bigelow, W.; Voyles, P.; Allard, L. *Catal. Lett.* **2012**, *142*, 176–182.
- (120) Venables, J. A. *Surf. Sci.* **1994**, *299–300*, 798–817.
- (121) de Resende, N. S.; Eon, J.-G.; Schmal, M. *J. Catal.* **1999**, *183*, 6–13.
- (122) Shang, J.; Gao, X. *Chem. Soc. Rev.* **2014**, *43*, 7267–7278.
- (123) Akdogan, Y.; Vogt, C.; Bauer, M.; Bertagnolli, H.; Giurgiu, L.; Roduner, E. *Phys. Chem. Chem. Phys.* **2008**, *10*, 2952–2963.
- (124) Chakarova, K.; Mihaylov, M.; Hadjiivanov, K. *Microporous Mesoporous Mater.* **2005**, *81*, 305–312.
- (125) Chakarova, K.; Hadjiivanov, K.; Atanasova, G.; Tenchev, K. *J. Mol. Catal. A: Chem.* **2007**, *264*, 270–279.
- (126) Yamasaki, Y.; Matsuoka, M.; Anpo, M. *Catal. Lett.* **2003**, *91*, 111–113.
- (127) Stakheev, A. Y.; Shpiro, E. S.; Tkachenko, O. P.; Jaeger, N. I.; Schulz-Ekloff, G. *J. Catal.* **1997**, *169*, 382–388.
- (128) Bischoff, H.; Jaeger, N. I.; Schulz-Ekloff, G.; Kubelkova, L. *J. Mol. Catal.* **1993**, *80*, 95–103.
- (129) Primet, M.; Basset, J. M.; Mathieu, M. V.; Prettre, M. *J. Catal.* **1973**, *29*, 213–223.
- (130) Hadjiivanov, K.; Saint-Just, J.; Che, M.; Tatibouet, J.-M.; Lamotte, J.; Lavalley, J.-C. *J. Chem. Soc., Faraday Trans.* **1994**, *90*, 2277–2281.
- (131) Hadjiivanov, K. I. *J. Chem. Soc., Faraday Trans.* **1998**, *94*, 1901–1904.
- (132) Mihaylov, M.; Chakarova, K.; Hadjiivanov, K.; Marie, O.; Daturi, M. *Langmuir* **2005**, *21*, 11821–11828.
- (133) Kustov, L. M.; Sachtler, W. M. H. *J. Mol. Catal.* **1992**, *71*, 233–244.
- (134) Zholobenko, V. L.; Lei, G.-D.; Carvill, B. T.; Lerner, B. A.; Sachtler, W. M. H. *J. Chem. Soc., Faraday Trans.* **1994**, *90*, 233–238.
- (135) Ding, K.; Gulec, A.; Johnson, A. M.; Schweitzer, N. M.; Stucky, G. D.; Marks, L. D.; Stair, P. C. *Science* **2015**, *350*, 189–192.
- (136) Panagiotopoulou, P.; Christodoulakis, A.; Kondarides, D. I.; Boghosian, S. *J. Catal.* **2006**, *240*, 114–125.
- (137) Resende, N.; Perez, C.; Eon, J.; Schmal, M. *Catal. Lett.* **2011**, *141*, 1685–1692.
- (138) Jackson, S. D.; Willis, J.; McLellan, G. D.; Webb, G.; Keegan, M. B. T.; Moyes, R. B.; Simpson, S.; Wells, P. B.; Whyman, R. *J. Catal.* **1993**, *139*, 191–206.
- (139) Shyu, J. Z.; Otto, K. *Appl. Surf. Sci.* **1988**, *32*, 246–252.
- (140) Schneider, W.-D.; Laubschat, C. *Phys. Rev. B: Condens. Matter Mater. Phys.* **1981**, *23*, 997–1005.
- (141) Davis, L. E.; Palmberg, P. W.; Riach, G. E.; Weber, R. E. *Handbook of Auger Electron Spectroscopy*, 2nd ed.; Physical Electronics Division, Perkin-Elmer Corporation: 6509 Flying Cloud Drive, Eden Prairie, MN 55343, 1978.
- (142) Zhang, C.; Liu, F.; Zhai, Y.; Ariga, H.; Yi, N.; Liu, Y.; Asakura, K.; Flytzani-Stephanopoulos, M.; He, H. *Angew. Chem., Int. Ed.* **2012**, *51*, 9628–9632.
- (143) Arroyo-Ramirez, L.; Chen, C.; Cargnello, M.; Murray, C. B.; Fornasiero, P.; Gorte, R. J. *J. Mater. Chem. A* **2014**, *2*, 19509–19514.
- (144) Rodriguez, J. A.; Kuhn, M. *J. Chem. Phys.* **1995**, *102*, 4279–4289.
- (145) Iwasa, N.; Mayanagi, T.; Ogawa, N.; Sakata, K.; Takezawa, N. *Catal. Lett.* **1998**, *54*, 119–123.
- (146) Iwasa, N.; Takezawa, N. *Top. Catal.* **2003**, *22*, 215–224.
- (147) Pangborn, A. B.; Giardello, M. A.; Grubbs, R. H.; Rosen, R. K.; Timmers, F. *J. Organometallics* **1996**, *15*, 1518–1520.
- (148) Some fluoride contamination was found on these materials, likely from decomposition of perfluorinated grease contaminants during the calcination process. Perfluorinated greases were used in various steps of the syntheses of the organometallic compounds and the supported organometallic complex.
- (149) Elam, J. W.; Groner, M. D.; George, S. M. *Rev. Sci. Instrum.* **2002**, *73*, 2981–2987.
- (150) Mudrakovskii, I. L.; Shmachkova, V. P.; Kotsarenko, N. S.; Mastikhin, V. M. *J. Phys. Chem. Solids* **1986**, *47*, 335–339.
- (151) Schneider, C. A.; Rasband, W. S.; Eliceiri, K. W. *Nat. Methods* **2012**, *9*, 671–675.
- (152) Anderson, J. R. *Structure of metallic catalysts*; Academic Press: London, New York, 1975.
- (153) Rioux, R. M.; Song, H.; Hoefelmeyer, J. D.; Yang, P.; Somorjai, G. A. *J. Phys. Chem. B* **2005**, *109*, 2192–2202.